applied optics

Angle of sky light polarization derived from digital images of the sky under various conditions

Wenjing Zhang,[1] Yu Cao,[2] Xuanzhe Zhang,[1] Yi Yang,[1] and Yu Ning[1,*]

[1]College of Optoelectronic Science and Engineering, National University of Defense Technology, Changsha 410073, Hunan, China
[2]College of Aerospace Science and Engineering, National University of Defense Technology, Changsha 410073, Hunan, China
*Corresponding author: ningyu_0205@126.com

Received 28 October 2016; revised 24 November 2016; accepted 24 November 2016; posted 15 December 2016 (Doc. ID 279742); published 17 January 2017

Skylight polarization is used for navigation by some birds and insects. Skylight polarization also has potential for human navigation applications. Its advantages include relative immunity from interference and the absence of error accumulation over time. However, there are presently few examples of practical applications for polarization navigation technology. The main reason is its weak robustness during cloudy weather conditions. In this paper, the real-time measurement of the sky light polarization pattern across the sky has been achieved with a wide field of view camera. The images were processed under a new reference coordinate system to clearly display the symmetrical distribution of angle of polarization with respect to the solar meridian. A new algorithm for the extraction of the image axis of symmetry is proposed, in which the real-time azimuth angle between the camera and the solar meridian is accurately calculated. Our experimental results under different weather conditions show that polarization navigation has high accuracy, is strongly robust, and performs well during fog and haze, clouds, and strong sunlight.

OCIS codes: (110.1758) Computational imaging; (280.4788) Optical sensing and sensors; (110.7348) Wavefront encoding; (110.5405) Polarimetric imaging; (010.1310) Atmospheric scattering.

https://doi.org/10.1364/AO.56.000587

1. INTRODUCTION

Sunlight becomes polarized because of Rayleigh scattering [1–3]. When transmitting in the atmosphere, it forms a special polarization pattern: the polarized e-vector direction is perpendicular to the plane determined by the sun, the point observed on the celestial sphere, and the position of the observer. Thus it can be seen that the characteristic of this polarization distribution has some relationship with the direction of the sun and can be used for navigation. Compared with the existing multiform navigation methods, polarization navigation has many advantages: first of all, it is more robust than GPS [4,5] and earth magnetism navigation, which are easily disturbed by environment factors; second, it mainly relies on external reference to assist its navigation, which helps it avoid negative effects, such as the error cumulative effect in inertial navigation systems (INSs) [6,7]. From this point of view, it can provide higher accuracy even when operating over a long period of time. What is more, it is much cheaper than INS.

The difference between the polarization navigation and the sun sensor [8] is that although both of them fall into the category of celestial navigation, the former can operate under some adverse weather conditions such as fog, haze, and clouds when the sun cannot be observed directly.

Detecting the information of degree of polarization (DOP) and angle of polarization (AOP), which together are called the polarization pattern, precisely is the precondition for navigating with polarization. Existing technology [9–13] usually applies a digital camera and a wide-angle lens in detecting the sky light polarization pattern across a wide field of view. However, this method requires multiple images of the sky obtained with linear polarizers set at different angles. There are two ways to accomplish this task: one camera takes pictures at different times [9] (time-sharing measurement) or multiple cameras take pictures at the same time [11] (space-sharing measurement). Obviously, the former sacrifices real-time ability, and the latter induces extra complexities and a higher cost to the detecting system. The most severe problem is that existing methods for sky light polarization detection have a poor weather adaptability. Horváth *et al.* [1,14,15] made an in-depth research and analysis on the measurement accuracy for the sky light polarization pattern. The influence of fog and haze was also analyzed by Wu *et al.* [16] in 2015. Numerous experimental results [1,2,9,14–17] showed that clouds, sunlight, and haze would indeed have an effect on the measurement results and decrease the navigation precision. This is because the polarization information at each point is calculated by the exact value of pixel

gray in the image. Bad weather conditions and the imaging noise can easily cause error to the value of pixel gray, which is the main reason for the weak robustness in bad weather. Instead of relying on every single pixel gray, there are two ways to solve this problem: one is recording the sky light polarization information through the image texture feature [18], which is more resistant to interference. However, this method is still time consuming and impractical because of its inefficient algorithm. Another way also sacrifices the sampling resolution for its robustness. In this second method, the polarization value of an observed point in the sky can be calculated through a macro pixel, which is comprised of a group of multiple true pixels [19–21]. The algorithm for this method is simple, and it has a good real-time performance and an exciting application prospect.

There are also two solutions now to obtain the sky light polarization information regionally rather than pixel-for-pixel: one is to cover the surface of a charge coupled device (CCD) or complementary metal-oxide semiconductor (CMOS) with an array of micro polarizers [19,21], each element of which in the array covers multiple pixels. However, fabrication and installation for this kind of micro polarizer array is extremely complicated. This imposes many restrictions on its application. Another solution is proposed by this paper's author [20], which is based on the light field camera and lens coded aperture. The previous experimental results [20] gave a test for accuracy and real-time ability with this method. However, some problems remained: (1) the navigation angle has not been calculated with information of polarization, and (2) test experiments have not been conducted under different weather conditions.

Work in this paper is orientated toward these problems. After redrawing the image of AOP with a new reference coordinate system, the real-time azimuth angle between the carrier and the sun is obtained with the algorithm of the symmetry axis extraction in an image. Experimental results under different weather conditions show that the polarization navigation method in this paper has a strong robustness and good ability for bad weather resistance.

2. SKYLIGHT POLARIZATION DETECTION WITH LIGHT FIELD CAMERA

In our previous work [20], the imaging system for sky light polarization detection is based on a polarizer triplet and a light field camera with a micro lens array before the sensor plane. Figure 1 is the principle diagram of the system. The polarizer triplet is placed at the lens aperture. The subimage after each micro lens is the image of the main lens, which is divided into three regions. When the incident light is unpolarized, the pixel gray values in three adjacent parts of every subimage are the same, whereas when the incident light is polarized, they are related to the different transmittances of the three parts, as shown in Fig. 1. With this optical structure, the light intensity from the arbitrary viewpoint of the sky is modulated by polarizers orientated to three different directions. From each viewpoint, the three levels of the skylight intensity can be obtained in a single shot. This information then can be used for calculating the polarization pattern (AOP and DOP) with Stokes' equations [22].

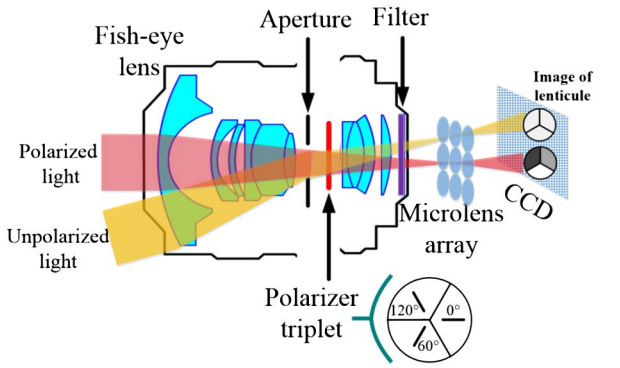

Fig. 1. Schematic diagram of detection system principle for the sky light polarization pattern based on light field camera.

The Stokes vector S contains 4 components: $S = [I, Q, U, V]$. By tuning the polarizer in direction at 0°, 60°, and 120°, we can get three light intensity outputs, marked as $I_{0°}$, $I_{60°}$, $I_{120°}$, respectively. In our system [20], values of $[I, Q, U]$ can be obtained with the following Eq. (1):

$$\begin{cases} I = \frac{2}{3}(I_{0°} + I_{60°} + I_{120°}) \\ Q = \frac{2}{3}(2I_{0°} - I_{60°} - I_{120°}) \\ U = \frac{2}{\sqrt{3}}(I_{60°} - I_{120°}) \end{cases}. \tag{1}$$

Then the sky light polarization pattern can be computed with the following Eqs. (2) and (3). Because the circularly polarized component of skylight could be negligible [16], V in Eq. (2) is zero:

$$\mathrm{DOP} = \frac{\sqrt{Q^2 + U^2 + V^2}}{I} = \frac{\sqrt{Q^2 + U^2}}{I}, \tag{2}$$

$$\mathrm{AOP} = \frac{1}{2}\arctan\left(\frac{U}{Q}\right). \tag{3}$$

3. REDRAWING AOP IMAGE AND POLARIZATION NAVIGATION METHOD

A. Redrawing of AOP Image

The sky light polarization pattern includes AOP and DOP. It is well accepted that more information of the sun direction is contained in AOP, which is more advantageous in resisting the influence of clouds. As a result, our research work in the following paragraph is more focused on the distribution of the AOP.

The reference start direction of the exact value of AOP is defined as the 0° orientation of a linear polarizer triplet. In this way, the obtained AOP data across the entire sky shows a characteristic called inverse symmetry distribution, as in Fig. 2, which is one of the measurement results of our imaging system. Different values of AOP are distinguished by different colors. The horizontal line stands for the solar meridian and indicates the direction of the sun with its arrow. The inverse symmetry means that values in the region of A and B are almost the same, as are regions C and D.

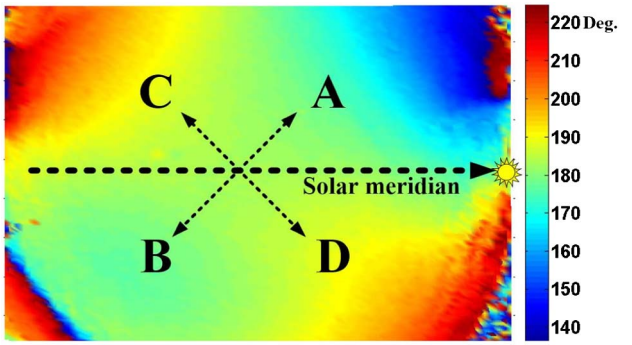

Fig. 2. Calculated result of the AOP on clear day.

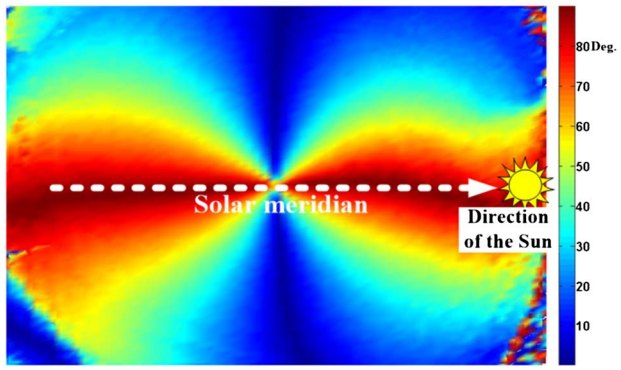

Fig. 4. Result redrawing map of Fig. 2.

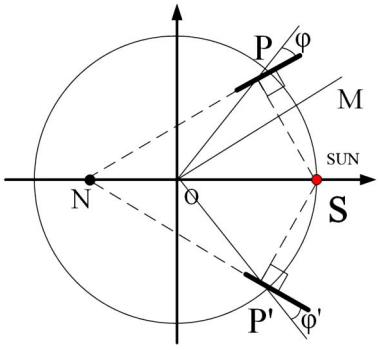

Fig. 3. Schematic diagram of redrawing method for AOP image.

It is clear that the solar meridian cannot be visualized easily in the map with inverse symmetry. So it is necessary to change the reference direction for AOP calculation and redraw the AOP image to visualize its symmetrical characteristic with respect of the sun meridian. The calculation model for redrawing is explained more clearly with the diagram which is shown in Fig. 3.

This is a two-dimensional (2D) projection of the 3D coordinates of the celestial sphere. The projection of the zenith is point O. Assuming that the elevation of the sun is 0°, at this time the horizontal coordinate axis is the projection line of the solar meridian. Point S stands for the position of the sun. Take two points, P and P', for example, which are symmetrical to the solar meridian. OM is the base line defined at random with respect to which to calculate the value of AOP. Actually, this direction is chosen according to the polarization direction of the linear polarizer. According to the Rayleigh scattering theory, $NP \perp SP$ and $NP' \perp SP'$. The angle between NP and OP and the angle between NP' and OP' are geometrically symmetrical with respect to the line of the sun meridian. However, if we calculate AOP with respect to the orientation OM, it is clear that $\measuredangle MOP \neq \measuredangle MOP'$ in most conditions. That is why the symmetrical axis (solar meridian) of the distribution map of AOP cannot be shown clearly if the starting line for AOP calculation is fixed. In other words, this kind of AOP distribution image shows little symmetry. Therefore, we redraw the image of AOP distribution with a new reference coordinate: For each observed point in the sky, the starting direction from which to calculate the value of polarization angle is the line going through the point itself and the original point O. In this way the reference direction varies according to different observation points. The relative value of the polarization angle at one point is defined as the acute angle between the scattering light orientation at this exact point and the reference direction.

Figure 4 shows the result of redrawing the map of Fig. 2 using the method described above. The symmetric characteristic about the sun meridian in the redrawn map of AOP has been seen clearly, and values of the calculated polarization angle along the sun meridian line are approaching 90°. This means the angle of polarization is 90° at these points. It matches the theoretical prediction [1–3] well, which lays the foundation for our work of extracting the course angle in the next step.

B. Polarization Navigation Method

First, we should extract the sun meridian in order to get the value of the course angle. This means the axis of symmetry in Fig. 4 should be obtained. There are mainly two kinds of methods to get the symmetrical axis in an image: one is based on principal component analysis [23] and the other is based on the image's phase information [24]. Some complicated and accuracy limited work such as boundary detection, image filtering, and noise reduction are required in the principal component analysis method. With the latter method based on the image's phase information, although some image preprocess work is not needed, multiple redundant lines of symmetrical axis may emerge. In 2015, Lu *et al.* [25] extracted the line of the solar meridian in the image of AOP with the Hough transform algorithm. However, only a small part of the image area was utilized, which caused a weak robustness. In the same year, a method for solar meridian extraction based on symmetry characteristic evaluation in the AOP image was proposed by Ma *et al.* [26]. This method has the capability to reduce the influence of clouds to some extent. Recently, a novel method based on a pulse coupled neural network algorithm for the highly accurate and robust compass information calculation from the polarized skylight imaging has been proposed by Tang *et al.* [17], which has shown good accuracy and reliability.

For the special symmetric characteristic of the sky light polarization image, a new method to detect the symmetric axis in

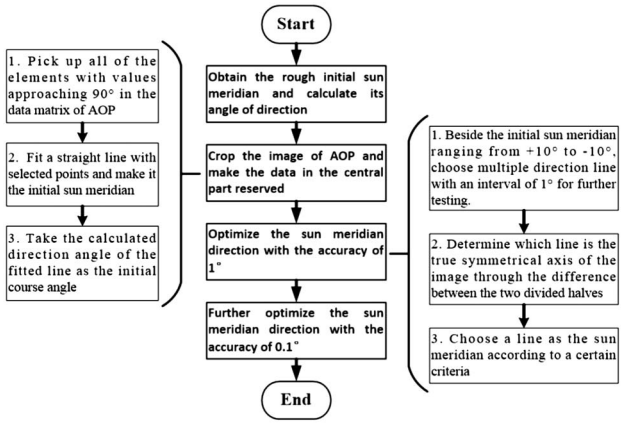

Fig. 5. Flow chart for course angle calculation with AOP image.

an image accurately and quickly is proposed without image preprocessing. Additionally, it has a strong ability of interference resistance. Figure 5 is the work flow of this method going through four main steps and the subflow chart within some key steps is also included with detail.

As we have obtained the redrawn map of the AOP image and visualized its obvious symmetry with the method in the previous Section 3.A, all of the following operations are conducted upon these redrawn images. First, roughly determine the symmetrical axis of obtained images. It is completed by picking up discrete points whose exact value is about 90°. Fit a line to these selected points, and make its slope the initial course angle. In order to make full use of the total points in the image, image cropping is implemented, and only the round central part data is reserved for further processing. It should be noted that this step can be skipped if a circular fish eye lens is employed whose image is round. Then we select several alternative lines beside the initial one with an interval of 1°. For each of them, we test whether it is the ideal symmetrical axis by subtracting the two halves of the round image segmented by it. The different images after subtracting by two different axes are listed in Fig. 6. For example, in Fig. 6(a), line A and line B are two alternative axes. The average gray value of Fig. 6(c) is less than that of Fig. 6(b), which means the axis used for the right image is closer to the true symmetrical axis. The ultimate course angle can be calculated and confirmed by comparing the image symmetry along different axes.

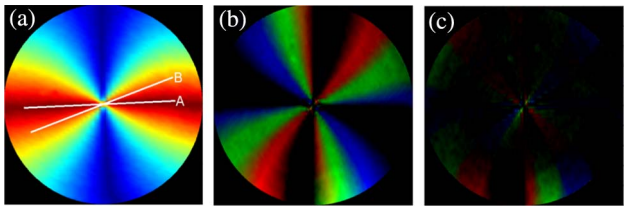

Fig. 6. (a) AOP image after cropping. Only the central part is reserved. (b) AOP mage after subtracting two halves of (a) along line B. (c) AOP image after subtracting two halves of (a) along line A.

4. EXPERIMENTAL AND RESULT ANALYSIS

Experiments were carried out on the roof of a building of the National University of Defence Technology. The resolution of the light field camera (type: Raytrix-R29) is 6576 × 4384. The micro lens array has 205 × 137 micro lenses, and each of them covers 32 × 32 pixels beneath. The wide-angle lens is from Zenitar, whose diagonal field of view is about 165°, and its focal length is 16 mm. The light field camera was fixed at a turntable with precise scale, with which the obtained course angle accuracy can be tested quantitatively. Figure 7 is our experimental platform, which is also described in [20] in detail.

A variety of experiments were carried out under different daytime weather conditions such as clear, cloudy, foggy, and hazy to test the precision and performance of our method and system. Figure 8 shows photos of these different weather conditions and includes brief descriptions. It should be noted that Figs. 8(b) and 8(c) were taken at different times of one day. Figure 8(b) was taken at the brief moment when the sun came out through the clouds to highlight the occlusion effect of the haze and fog.

A. Experimental Results under Clear Weather

Theoretically, the degree of polarization is much higher in a clear sky, when the measurement results of the polarization pattern should be more accurate. In this section the experiment was carried out with the camera being stationary. The camera took four images of the sky every 4 min without movement. Because of the same time interval, the theoretical variation of the sun direction between every two consecutive images is also almost the same. Thus the accuracy of the course angle obtained can be evaluated quantitatively through the differences between the four frames of image.

Figure 9 gives the photograph of the sky, the image of AOP, and the calculated value of the course angle. Because the time interval is only about 4 min, and it is known that the azimuth angle of the sun changes 15° each hour, the theoretical variation of the sun direction between every two consecutive images is about 0.5° according to our time and location. The variation is so small that it is hardly distinguished by human eyes. However, it is exciting that each resulting image is rotated slightly in the same direction and the angle variation between

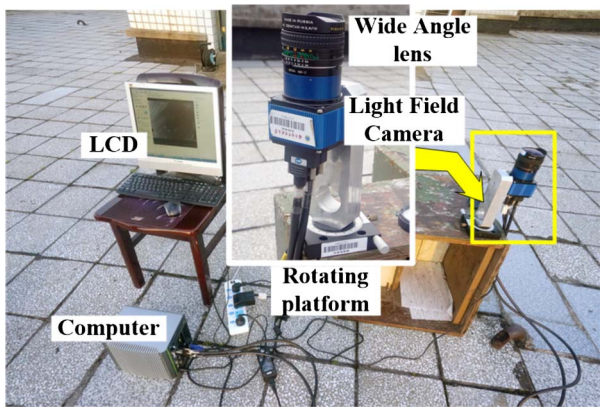

Fig. 7. Photograph of our experiment scene. The magnified area shows the compact and portable imaging equipment.

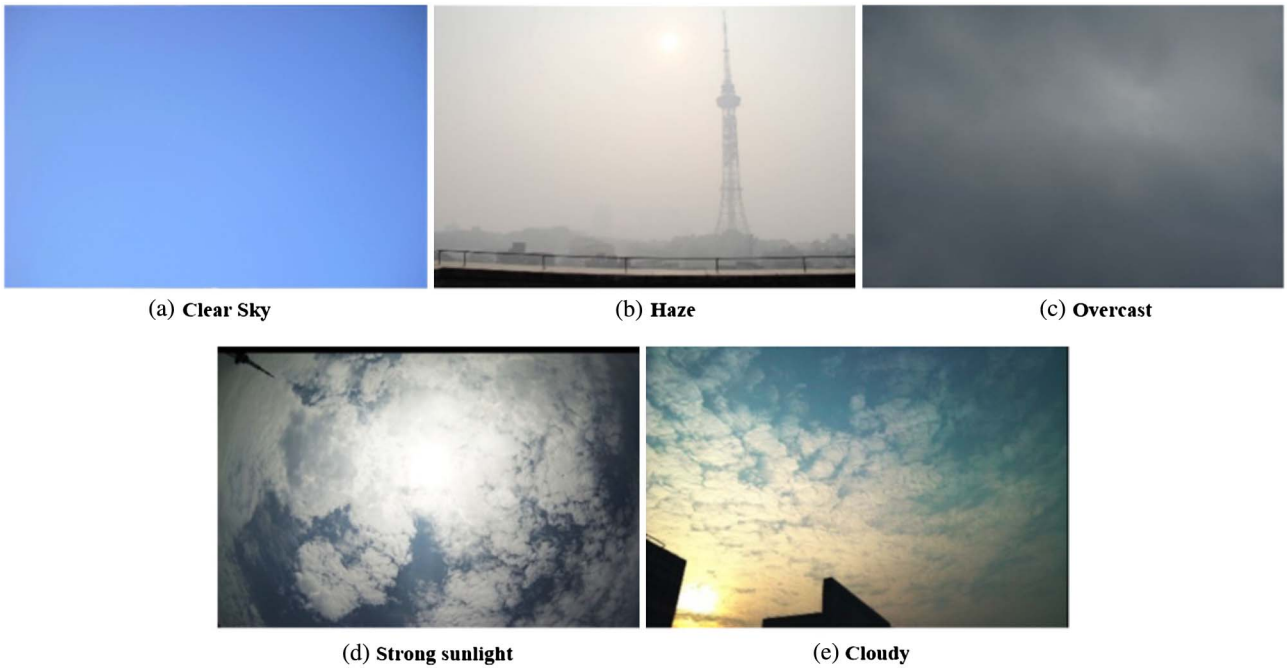

Fig. 8. Photographs of the sky under different weather conditions.

every two adjacent images matched well with the estimated value of 0.5°. So this experiment indicated that the method in this paper gave an accurate result of course angle.

B. Experimental Results under Sunny Weather

A wide angle lens was used to acquire the sky light polarization pattern across a large field of view. Therefore it was inevitable

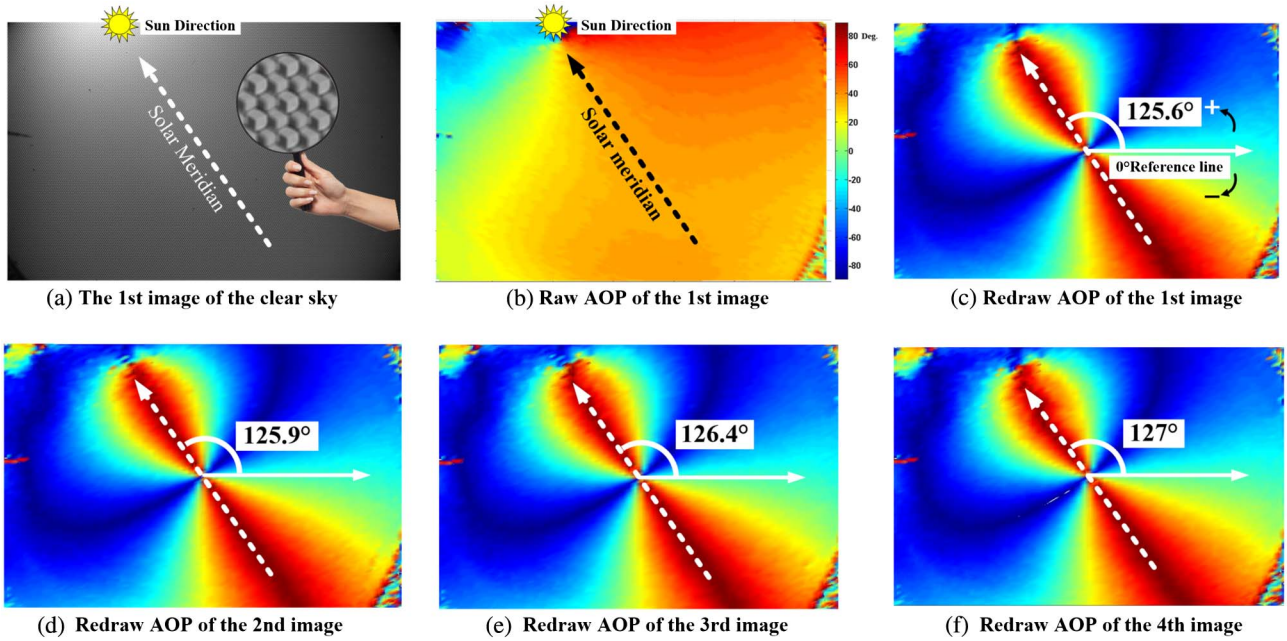

Fig. 9. Experiment results in a clear sky. (a) Original photograph taken by the light field camera. It can be seen from the magnified part that every subimage behind the micro lens is the image of the linear polarizer triplet mounted at the lens aperture, which has been divided into three parts with different pixel gray. (b) is the raw image of AOP data; (c) is the redrawn image of (b). The symmetric feature of the polarization pattern with respect to the sun meridian is shown clearly. We defined the horizontal rightward direction as the reference direction of 0° and counterclockwise rotation as positive for the course angle calculation. (d)–(f) are three other images of experimental results with the same time interval, and the calculated values of course angle are labeled.

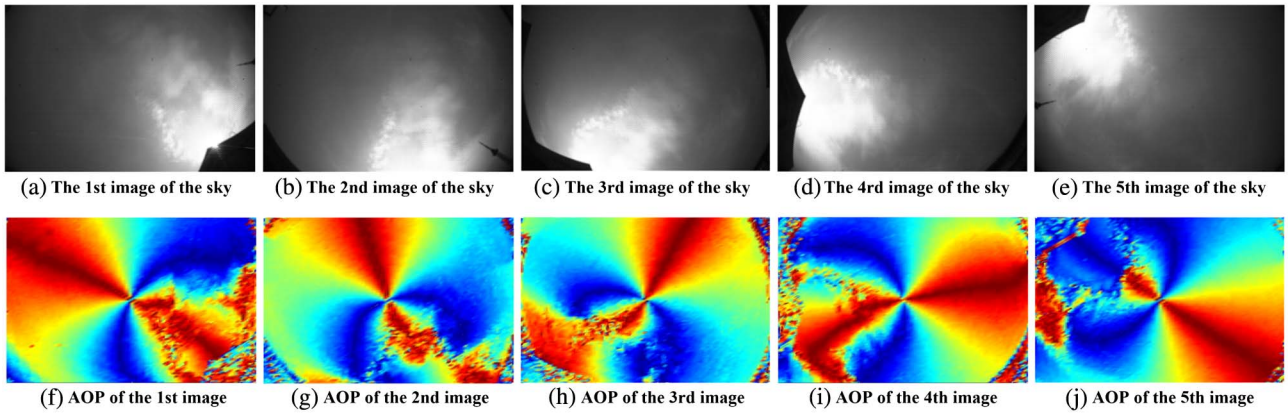

Fig. 10. Overexposed image sequence of the sky taken by the light field camera and corresponding calculated AOP results calculated.

that the sun emerged in the imaging field and brought about overexposure and information loss, which resulted in negative effects on the measurement of the sky light polarization. So the following experiments were conducted to test the accuracy and robustness of our system in this condition.

The camera was erected vertically to take five photos of the sky with different rotation angles. Figure 10 gives the raw pictures and redrawn maps of AOP. As can been seen from Fig. 10, pixels around the sun are overexposed. So data there is influenced greatly and cannot provide any useful information for calculating polarization. However, the overall symmetric feature of the image with respect to the sun meridian is kept well and still can be recognized easily.

Table 1 shows the actual course angle and the calculated results. We can see that the errors increase under this condition. This experiment shows that image overexposure will influence the measurement accuracy.

C. Experimental Results under Cloudy Weather

The polarized components of the sky light are mainly caused by the light scattered by gas molecules in the upper atmosphere. So the existence of clouds disturbs the collection of the scattered sky light in a polarization imaging system and thus affects the navigation accuracy. Therefore, it is necessary to analyze the impact on the accuracy of both polarization measurement and course angle extraction under cloudy weather.

Figure 8(e) is the photo of cloudy weather. Nearly half the sky was covered by clouds, which resulted in a steep change in the brightness of the image. It happened that clouds were distributed along one side of the sun meridian. So it was beneficial for us to analyze the influence of the clouds to the sky light polarization measurement. Figure 11 is the group of three experimental images and the corresponding measurement results of AOP. The time interval between them is less than 10 s. Therefore, course angle variation due to the sun's movement can be neglected. The sun's different positions within the three images were caused by the camera's rotation. As can be seen easily from the distribution image of AOP, the existence of clouds indeed brought corrugated error to the measurement. This might influence the accuracy of the final course angle calculation results to some extent.

Table 2 lists values of true course angles and their corresponding calculated ones of the three frames of image. The results reveal that clouds produce some influence on the course angle calculation with an error of 1° or so.

Table 1. Comparison between the True Course Angles and the Calculated Angles When the Camera Was Disturbed by Strong Sunlight

Image No.	True Value (°)	Calculated Value (°)	Error (°)
1	−27°	−27.5°	0.5°
2	−73°	−70.8°	−2.2°
3	−118°	−118.8°	0.8°
4	−172°	−170.7°	−1.3°
5	145.5°	146°	−0.5°

D. Experimental Results under Overcast and Haze Weather

The previous experimental results show that, with our sky light polarization detection system based on the light field camera, measurement results are more accurate in clear conditions. Additionally, the extracted course angle also has a higher precision. Compared with the sun sensor, the most advantageous and different point for the sky light polarization navigation method is its applicability when the sun cannot be seen (e.g., in cloudy conditions or foggy and hazy weather). Thus this necessitates a test for course angle extraction precision in those severe weather conditions with our method.

Cloud overcast, fog, and haze fall into different types of weather conditions. However, they have some common effects for our detection system: first, the sky is fully covered and the clouds, fog, and haze are usually in a lower altitude atmosphere. Therefore the detection system has difficulty receiving the light scattered by upper gas molecules. This requires the system to have a higher sensitivity for polarization detection. Second, the sky light is uniform, and there is no obvious texture in the image of the sky. This test experiment was conducted on a overcast day with severe fog and haze. The PM2.5 reading was 175, belonging to heavy pollution grade, when the sky was totally covered by clouds, fog, and haze, as shown by Figs. 8(b) and

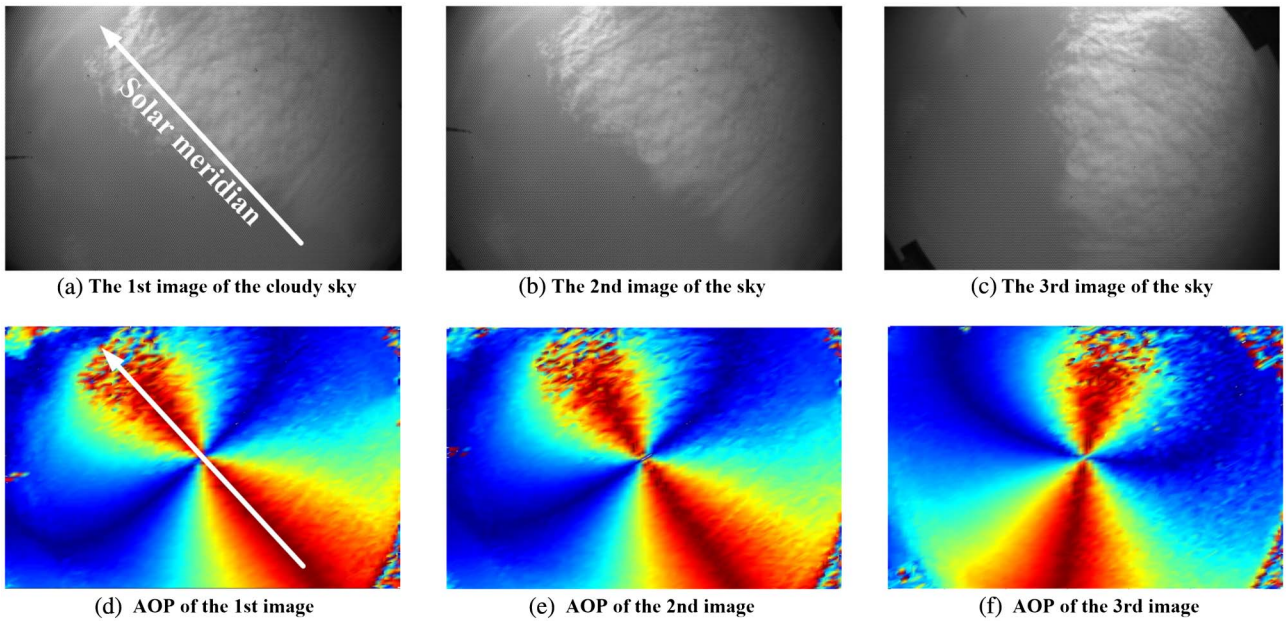

Fig. 11. Three experimental photographs of the sky, including their corresponding AOP distribution images, taken in cloudy condition under different rotation angles of the camera.

Table 2. Values of True Course of Angle and the Calculated Angle in Cloud Cover

Image No.	True Value (°)	Calculated Value (°)	Error (°)
1	132.5°	133.1°	−0.6°
2	125.5°	125.2°	0.3°
3	78.5°	79.4°	−0.9°

8(c). Figure 12 is the picture of the sky taken by the light field camera and the corresponding polarization pattern image. Because the sun was totally occluded by clouds, the exact direction of the sun cannot be recognized with the naked eye and was not marked in Fig. 12(a). Figure 12(b) is the result of DOP. The DOP was so low that its symmetrical distribution characteristic with respect to the sun meridian, depicted by the Rayleigh theory, utterly cannot be recognized. Fig. 12(c) is the image of AOP distribution. The obtained sun meridian was indicated by the white arrow, the direction of which approximately matched with the orientation of the sun. Thus we can conclude that clouds, fog, and haze can occlude the polarized light from Rayleigh scattering in the sky and produce large error to the polarization pattern detection.

A further experiment was carried out to test the accuracy of course angle extraction in foggy and hazy weather. The camera was also erected vertically and took pictures at the frame rate of 0.5 fps. The rotary table was rotating simultaneously with a step increment of 2° between every two adjacent pictures. Then we calculated the image of AOP from each picture of the sky and extracted its course angle. Figure 13 is the chart plotted according to the results in this experiment and describes the changing of course angle values. The upper blue line reveals the actual course angle varying with image sequence, and the bottom line is the calculated result. Although the calculated result drops to smaller values compared with the true ones, the increase trend of the calculated course angle is correct. However, the exact values are smaller than the real ones in this weather condition. The main reason for the error is the severe weather condition, and another reason may be the uncorrected distortion of the wide angle lens.

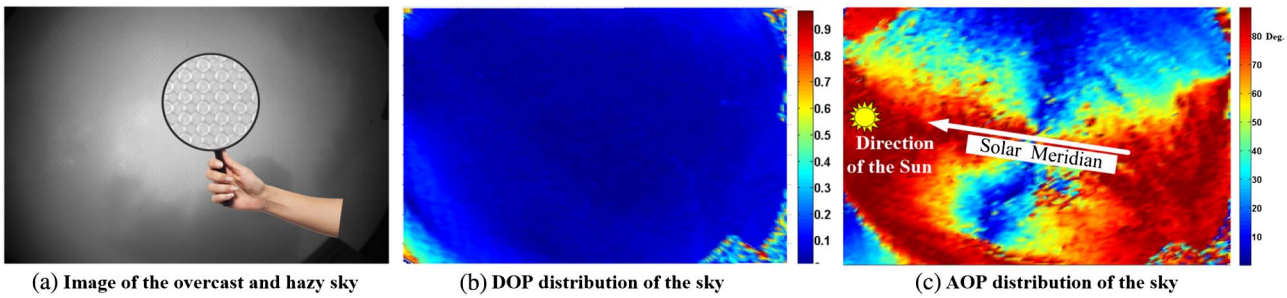

Fig. 12. Photograph of the overcast and hazy sky taken by the light field camera and its corresponding result of polarization pattern.

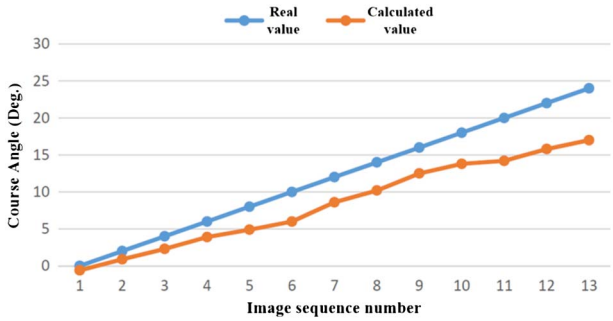

Fig. 13. Comparison curves between the true and calculated course angles.

5. CONCLUSION AND FUTURE WORK

This paper shows research on how to obtain course angle with the information of sky light polarization pattern distribution and proposed an algorithm for the angle extraction through searching for the symmetry axis of an image. Large quantities of experiments exhibited precision performance with this method. Some conclusions can be drawn as follows: first, the course angle can be obtained with sky light polarization pattern information accurately in a clear sky. Second, the accuracy will be influenced by strong sunlight and clouds. However, an obvious symmetrical distribution characteristic of AOP and the value of the course angle can also be obtained in bad weather conditions, such as sunlight overexposure and cloud cover. The angle error is about 2°. Third, even in haze and fog, when the degree of polarization is low, a rough orientation of the sun meridian can still be detected.

The existing problems and further improvement are discussed as follows: first, the hardware of the system requires further optimization. The fish-eye lens in our system has a limited field of view. A circular fish eye lens which covers a larger circle field of the whole sky is better for our experiment. Besides, the light field camera in our system is designed and fabricated for 3D imaging, which is not suitable for sky light polarization detection. For instance, the micro lens array in the light field camera is comprised of three groups of micro lenses with different focal lengths in order to extend the imaging depth of field. As a result, two-thirds of the images of the sky are blurred. In addition, the dynamic range of this camera is relatively low, which leads to a poor exposure effect. Therefore, a customized light field camera is necessary according to the special application requirement.

Second, experimental methods should be improved. The fish-eye lens has a serious imaging distortion, which resulted in severe imaging deformation in our sky light polarization detection results. Therefore in our future work on polarization navigation, lens distortion will be bound to correct for a higher navigation accuracy.

Finally, it can be found from our experimental results that the robustness in our existing measurement method can be further enhanced, especially on cloudy days and days of strong sunshine when the accuracy decreases greatly. We will make an analysis of these problems and search for the best solution from a new perspective.

Funding. China Postdoctoral Science Foundation (2014m562649); National Natural Science Foundation of China (NSFC) (11504424, 61378065, 61505257).

Acknowledgment. The authors thank Ian for his modification of the article.

REFERENCES

1. B. Suhai and G. Horváth, "How well does the Rayleigh model describe the e-vector distribution of skylight in clear and cloudy conditions? a full-sky polarimetric study," J. Opt. Soc. Am. A **21**, 1669–1676 (2004).
2. G. Können, *Polarized Light in Nature* (CUP Archive, 1985).
3. M. Berry, M. Dennis, and R. Lee, Jr., "Polarization singularities in the clear sky," New J. Phys. **6**, 162 (2004).
4. P. Misra and P. Enge, *Global Positioning System: Signals, Measurements and Performance*, 2nd ed. (Ganga-Jamuna, 2006).
5. T. Aycock, A. Lompado, T. Wolz, and D. Chenault, "Passive optical sensing of atmospheric polarization for GPS denied operations," Proc. SPIE **9838**, 98380Y (2016).
6. F. Evennou and F. Marx, "Advanced integration of wifi and inertial navigation systems for indoor mobile positioning," EURASIP J. Appl. Signal Process. **2006**, 1–12 (2006).
7. R. Jin, H. Sun, J. Sun, W. Chen, and J. Chu, "Integrated navigation system for uavs based on the sensor of polarization," in *IEEE International Conference on Mechatronics and Automation (ICMA)* (IEEE, 2016), pp. 2466–2471.
8. A. Trebi-Ollennu, T. Huntsberger, Y. Cheng, E. T. Baumgartner, B. Kennedy, and P. Schenker, "Design and analysis of a sun sensor for planetary rover absolute heading detection," IEEE Trans. Rob. Autom. **17**, 939–947 (2001).
9. Y. Wang, X. Hu, J. Lian, L. Zhang, Z. Xian, and T. Ma, "Design of a device for sky light polarization measurements," Sensors **14**, 14916–14931 (2014).
10. M. Sarkar, D. S. S. Bello, C. Van Hoof, and A. Theuwissen, "Biologically inspired autonomous agent navigation using an integrated polarization analyzing CMOS image sensor," Procedia Eng. **5**, 673–676 (2010).
11. D. Wang, H. Liang, H. Zhu, and S. Zhang, "A bionic camera-based polarization navigation sensor," Sensors **14**, 13006–13023 (2014).
12. M. Gecevičius, M. Beresna, and P. G. Kazansky, "Polarization sensitive camera by femtosecond laser nanostructuring," Opt. Lett. **38**, 4096–4099 (2013).
13. D. Miyazaki, M. Ammar, R. Kawakami, and K. Ikeuchi, "Estimating sunlight polarization using a fish-eye lens," IPSJ Trans. Comput. Vis. Appl. **1**, 288–300 (2009).
14. I. Pomozi, G. Horváth, and R. Wehner, "How the clear-sky angle of polarization pattern continues underneath clouds: full-sky measurements and implications for animal orientation," J. Exp. Biol. **204**, 2933–2942 (2001).
15. G. Horváth, *Polarized Light and Polarization Vision in Animal Sciences* (Springer, 2014).
16. L. Wu, J. Gao, Z. Fan, and J. Zhang, "Measurements of skylight polarization: a case study in urban region with high-loading aerosol," Appl. Opt. **54**, B256–B265 (2015).
17. J. Tang, N. Zhang, D. Li, F. Wang, B. Zhang, C. Wang, C. Shen, J. Ren, C. Xue, and J. Liu, "Novel robust skylight compass method based on full-sky polarization imaging under harsh conditions," Opt. Express **24**, 15834–15844 (2016).
18. W. Zhang, X. Zhang, Y. Cao, H. Liu, and Z. Liu, "Robust sky light polarization detection with an s-wave plate in a light field camera," Appl. Opt. **55**, 3518–3525 (2016).

19. J. Chang, H. He, C. He, and H. Ma, "DofP polarimeter based polarization microscope for biomedical applications," Proc. SPIE **9707**, 97070W (2016).
20. W. Zhang, Y. Cao, X. Zhang, and Z. Liu, "Sky light polarization detection with linear polarizer triplet in light field camera inspired by insect vision," Appl. Opt. **54**, 8962–8970 (2015).
21. Z. Liu, R. Zhang, Z. Wang, L. Guan, B. Li, and J. Chu, "Integrated polarization-dependent sensor for autonomous navigation," J. Micro/Nanolithogr., MEMS, MOEMS **14**, 015001 (2015).
22. M. Born and E. Wolf, *Principles of Optics: Electromagnetic Theory of Propagation, Interference and Diffraction of Light* (Cambridge University, 1999).
23. J. Shlens, "A tutorial on principal component analysis," arXiv:1404.1100 (2014).
24. Z. Xiao, Z. Hou, C. Miao, and J. Wang, "Using phase information for symmetry detection," Pattern Recognit. Lett. **26**, 1985–1994 (2005).
25. H. Lu, K. Zhao, Z. You, and K. Huang, "Angle algorithm based on Hough transform for imaging polarization navigation sensor," Opt. Express **23**, 7248–7262 (2015).
26. T. Ma, X. Hu, L. Zhang, J. Lian, X. He, Y. Wang, and Z. Xian, "An evaluation of skylight polarization patterns for navigation," Sensors **15**, 5895–5913 (2015).